AIP Journal of Applied Physics

The nonlinear dynamics of tapping mode atomic force microscopy with capillary force interactions

N. Hashemi, H. Dankowicz, and M. R. Paul

Citation: Journal of Applied Physics **103**, 093512 (2008); doi: 10.1063/1.2913054
View online: http://dx.doi.org/10.1063/1.2913054
View Table of Contents: http://scitation.aip.org/content/aip/journal/jap/103/9?ver=pdfcov
Published by the AIP Publishing

The nonlinear dynamics of tapping mode atomic force microscopy with capillary force interactions

N. Hashemi,[1,a)] H. Dankowicz,[2] and M. R. Paul[1]
[1]*Department of Mechanical Engineering, Virginia Polytechnic and State University, Blacksburg, Virginia 24061, USA*
[2]*Department of Mechanical Science and Engineering, University of Illinois at Urbana-Champaign, Illinois 61801, USA*

(Received 21 January 2008; accepted 27 February 2008; published online 6 May 2008)

We study the nonlinear dynamics of a tapping mode atomic force microscope with tip-surface interactions that include attractive, repulsive, and capillary force contributions using numerical techniques tailored for hybrid or discontinuous dynamical systems that include forward-time simulation with event handling and numerical pseudo-arclength continuation. We find four branches of periodic solutions that are separated by windows of complex and irregular dynamics. The branches of periodic solutions end where the cantilever comes into grazing contact with event surfaces in state space, corresponding to the onset of capillary interactions and the onset of repulsive forces associated with contact. These windows of irregular dynamics are found to coexist with the periodic branches of solutions as well as exist beyond the termination of the periodic solution. Finally, we show that these details can be overlooked unless one is careful to sample the dynamics appropriately. © *2008 American Institute of Physics*. [DOI: 10.1063/1.2913054]

I. INTRODUCTION

Atomic force microscopy (AFM) has been used extensively to study the surface topography of a wide variety of materials, and has also proven capable of measuring intramolecular forces.[1–3] When operating in tapping mode, the cantilever probe makes intermittent contact with the sample and, as a result, can be expected to reduce sample destruction during measurement as compared to contact modes. Consequently, the tapping mode has been widely employed to study compliant materials such as polymers, biomaterials, and semiconductors.[2,4] The interaction between the AFM probe tip and the sample is discontinuous or exhibits discontinuous changes in its rate of change with tip-sample separation, is hysteretic as in the presence of capillary interactions, and highly nonlinear. A substantial and growing literature is dedicated to the low-complexity modeling of these interactions and a study of their implications to the probe dynamics.[4–11]

Previous work has shown that, during tapping mode operation, the AFM probe dynamics explore two distinct branches of stable oscillations as one varies the equilibrium separation between the cantilever and the sample surface.[4,5] In the idealized absence of noise, transitions between these branches are found to be associated with the onset of repulsive tip-sample interactions when the cantilever comes into contact with the sample surface,[5] whereas premature transitions would be observed away from these conditions in the presence of noise. Zitzler *et al.*[6] explored the influence on these transitions of capillary forces, resulting from a thin layer of water on the sample and probe tip due to humidity in the surrounding air.

In this paper we study in detail the AFM dynamics using the model of Zitzler *et al.*[6] by developing and using specialized numerical algorithms that carefully treat the discontinuous and hysteretic spatial dependence of the force interactions between the cantilever tip and sample surface. While the theoretical tools particular to such hybrid systems are not detailed here (but can be found in the references), the resultant formalism avoids the introduction of additional model assumptions at the stage of numerical implementation of a forward-simulation model. Moreover, the hybrid formulation is associated with a well-defined algorithm for evaluating the dynamic stability of periodic system responses, as well as with techniques for tracing such responses under parameter variations regardless of their stability. In contrast to Zitzler *et al.*,[6] this paper therefore embraces the piecewise nature of the system definition and exploits this so as to plausibly explain complexities in the system response.

Hybrid dynamical systems form a natural backbone for the analysis of mechanical systems with impacts or dry friction (including conditions of stick or slip), electrical circuitry with nonlinear circuit elements, such as diodes and transistors, and biomolecular models with chemical switches, such as the mitotic halving of the cell mass (cf. Ref. 12). In these cases, as with the application considered here, and in contrast to smooth models, the hybrid formalism affords a means to accurately resolve changes in the system response that are directly associated with rapid changes in the system state or the state of system interactions.[13]

II. THE PHYSICAL MODEL

The atomic force microscope is composed of an elastic cantilever whose dynamics varies due to complex force interactions F_{ts} between the cantilever tip and the sample surface. Following Ref. 6, F_{ts} is assumed to include attractive long-range van der Waals forces F_v, capillary contributions

a)Electronic mail: nastaran@vt.edu.

F_c due to the presence of a liquid layer, and repulsive forces F_r representing the onset of contact. The objective of this section is to briefly outline the important model assumptions and quantitative expressions for each of these interactions. The reader is referred to Ref. 6 for further details.

Let d denote the instantaneous nominal tip-sample separation, i.e., the distance between the cantilever tip and a nominal reference plane associated with the sample surface. Assuming the interaction can be modeled as a sphere in close proximity to an infinite surface, the van der Waals forces are given by $F_v=HR/6d^2$ when $d>a_0$, where H is the Hamaker constant, R is the radius of curvature of the cantilever tip, and a_0 is the intermolecular constant. For separations $d\leq a_0$, the van der Waals force is assumed to be constant and equal to its value when $d=a_0$. The Derjaguin-Muller-Toporov (DMT) contact model[14] yields $a_0=(H/24\pi\gamma_{sv})^{1/2}$, where γ_{sv} is the surface energy of the tip and sample.

Contact between the cantilever tip and the sample surface, corresponding to $d<a_0$, is associated with a strong repulsive force. Again using DMT theory, this repulsive interaction is given by $F_r=-(4/3)E^*R^{1/2}(a_0-d)^{3/2}$, where $E^{*-1}=(1-\nu_t^2)/E_t+(1-\nu_s^2)/E_s$ and E_t,E_s,ν_t,ν_s are the Young's modulus and Poisson ratio for the tip (subscript t) and sample (subscript s), respectively.

The capillary force arises from the interactions between thin films of water of depth h that cover the sample and cantilever tip due to ambient humidity.[6,15–17] As the separation d falls below a critical distance $d_{\text{on}}=2h$, a connective column of liquid is established. Upon retracting away from the surface, the liquid column forms a meniscus and neck, until eventually breaking as the separation increases beyond a critical distance $d_{\text{off}}=V^{1/3}-V^{2/3}/5R$, where V is the meniscus volume. In the presence of the liquid column, the force interaction caused by the water layers can be modeled as $F_c=4\pi\gamma_w R/(1+d/h)$ when $d>a_0$, where γ_w is the surface energy of water. For separations $d\leq a_0$, the capillary force is assumed to be constant and equal to its value when $d=a_0$.

During tapping mode operation, a low-dimensional model reduction that provides a reasonably accurate description of the cantilever dynamics represents the cantilever by a lumped mass m that moves under the influence of a linear spring with stiffness k, a viscous damper with damping coefficient c, a harmonic driving with amplitude F_d and angular frequency ω_d (here assumed to equal the natural frequency $\omega_0=\sqrt{k/m}$), and the tip-sample interaction force F_{ts} discussed above. A schematic of such a model is shown in Fig. 1.

The corresponding equation of motion is now given by

$$m\ddot{q}+c\dot{q}+kq=F_d\cos\omega_d t+F_{ts}, \tag{1}$$

where $q=d_0-d$ is the instantaneous displacement of the cantilever tip measured from the equilibrium tip position in the absence of external forces (i.e., for an unstretched spring) with positive values toward the sample surface, and $\dot{q}$ and $\ddot{q}$ are the instantaneous velocity and acceleration, respectively, of the cantilever tip.

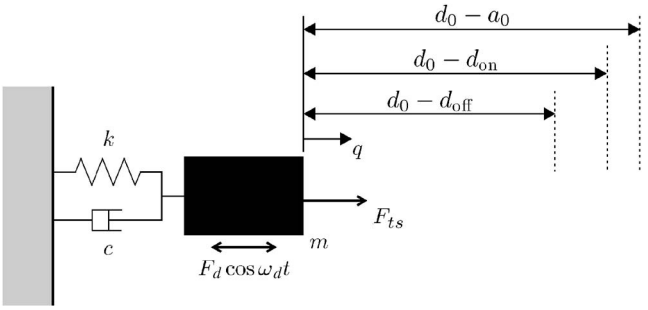

FIG. 1. A schematic of the lumped-mass model used to represent an AFM cantilever oscillating near a sample surface. The cantilever has mass m, spring constant k, and damping coefficient c. The cantilever is driven with a force of magnitude F_d and frequency ω_d. The interaction force F_{ts} captures the attractive, capillary, and repulsive interactions between the cantilever tip and the sample. The cantilever is shown at the equilibrium rest position which is at a distance d_0 from the sample surface. Also shown is the distance from the equilibrium rest position of the cantilever to the onset of the capillary force d_0-d_{on}, contact with the sample surface d_0-a_0, and the release of the capillary force d_0-d_{off}. The specific parameter values used in our numerical investigation are listed in Table II.

III. DISCUSSION

A. A hybrid dynamical system

The objective of this section is to recast the physical model discussed above as a *hybrid dynamical system* supporting a rigorous simulation formalism, within which the bifurcation characteristics of the atomic force microscope during tapping mode operation may be carefully explored.

Consider the three-dimensional continuous state vector $\mathbf{x}$ given by

$$\mathbf{x}=\begin{pmatrix}x_1\\x_2\\x_3\end{pmatrix}=\begin{pmatrix}q\\\dot{q}\\\omega_d t \bmod 2\pi\end{pmatrix}. \tag{2}$$

Here, x_1 and x_2 capture the mechanical state of the cantilever, while x_3 describes the instantaneous phase of the periodic driving. In addition to the continuous state vector $\mathbf{x}$, a complete description of the instantaneous state of the tip dynamics requires knowledge of the state of the tip-sample interactions, particularly the specific combination of tip-sample interaction forces that are active at a given moment. For this purpose, let i denote a discrete state variable, such that

$$F_{ts}(q,i)=\begin{cases}\dfrac{HR}{6(d_0-q)^2} & i=0\\[2ex] \dfrac{HR}{6(d_0-q)^2}+\dfrac{4\pi\gamma_{\text{H}_2\text{O}}R}{1+(d_0-q)/h} & i=1\\[2ex] \dfrac{HR}{6a_0^2}+\dfrac{4\pi\gamma_{\text{H}_2\text{O}}R}{1+a_0/h}-\dfrac{4}{3}E^*\sqrt{R}(a_0-d_0+q)^{3/2} & i=2\end{cases}. \tag{3}$$

In particular, $i=0$ corresponds to the state in which the tip-sample interaction force is entirely attractive and given by the van der Waals force. Similarly, $i=1$ corresponds to the state in which the tip-sample interaction force is a combination of attractive van der Waals and capillary force contribu-

TABLE I. An exhaustive list of all possible nondegenerate transitions between tip-sample interaction states as described by the index i, where i_b is the value of the index *before* the triggered event and i_a is the value of the index *after* the triggered event. Also shown are the event functions, h, for which a transversal zero crossing from positive to negative values triggers the indicated discrete change in the index variable.

i_b	i_a	h
0	1	d_0-q-d_{on}
1	0	$d_{\text{off}}-d_0+q$
1	2	d_0-q-a_0
2	1	a_0-d_0+q

tions. Finally, $i=2$ corresponds to the state in which the tip-sample interaction force is a combination of two attractive constant contributions (that equal the van der Waals and capillary force terms, respectively, when $d=a_0$) and a repulsive force contribution.

The dynamics of the AFM cantilever during tapping mode operation is captured through a combination of continuous-in-time evolution of the continuous state vector $\mathbf{x}$ as per the autonomous system of first-order differential equations,

$$\dot{\mathbf{x}} = \mathbf{f}(\mathbf{x},i) = \begin{pmatrix} x_2 \\ m^{-1}(F_d \cos x_3 - cx_2 - kx_1 + F_{ts}(x_1,i)) \\ \omega_d \end{pmatrix}, \quad (4)$$

and discrete-in-time changes of the discrete state variable i as per Table I.

Specifically, suppose that $i=0$ whenever $d_0-q>d_{\text{off}}$, and $i=2$ whenever $d_0-q<a_0$. Each row of Table I then corresponds to a transition between two distinct combinations of tip-sample interactions triggered by a transversal (i.e., nontangential) zero crossing of a characteristic event function from positive to negative values. In particular, let $h(\mathbf{x})$ be a function of the continuous state vector. Then, for a given value of the discrete state variable i, such a transversal zero crossing of the value of h along a system trajectory occurs at a time $t=t^*$ provided that

$$h[\mathbf{x}(t)]|_{t=t^*} = h[\mathbf{x}(t^*)] = 0 \quad (5)$$

and

$$\frac{d}{dt}h[\mathbf{x}(t)]\bigg|_{t=t^*} = \partial_{\mathbf{x}}h[\mathbf{x}(t^*)] \cdot \mathbf{f}[\mathbf{x}(t^*),i] < 0. \quad (6)$$

Here, $\partial_{\mathbf{x}}h$ denotes the gradient of the function h with respect to the components of the state vector $\mathbf{x}$, and the $\cdot$ denotes matrix multiplication.

Table I gives an exhaustive list of all possible nondegenerate transitions between distinct combinations of tip-sample interactions and the associated event functions. In particular, the change between $i_b=0$ and $i_a=1$ is associated with a discontinuous jump of $4\pi\gamma_w R/(1+d_{\text{on}}/h)$ in the tip-sample interaction force, corresponding to the onset of the capillary interactions. A similar discontinuous jump of $4\pi\gamma_w R/(1+d_{\text{off}}/h)$ in the tip-sample interaction force is associated with the transition between $i_b=1$ and $i_a=0$ and corresponds to the delayed rupture of the meniscus neck. In contrast, the transitions between $i_b=1$ and $i_a=2$ and vice versa are not associated with discontinuities in the tip-sample interaction force, although the gradient of the tip-sample interaction force is discontinuous across these transitions.

TABLE II. Values of the parameters used in the numerical analysis of the AFM cantilever dynamics. The cantilever is driven at the resonant frequency $\omega_d=\omega_0=2\pi f_0$, the equivalent mass of the cantilever is $m=k/\omega_0^2$, and the damping is given by $c=m\omega_0/Q$. The Hamaker constant $H=6.0\times10^{-20}$ J, the elastic modulus of the tip $E_t=120$ GPa, the Poisson coefficient of the tip $\nu_t=0.5$, the elastic modulus of the sample $E_s=120$ GPa, the Poisson coefficient of the sample $\nu_s=0.5$, the surface energy $\gamma_{sv}=75$ mJ/m^2, and the surface energy of water $\gamma_w=72$ mJ/m^2. For all of the results presented here, we have chosen F_d, which yields a free amplitude of oscillation of the cantilever to be $A_0=30$ nm.

Spring constant	k	27.5 N/m
Quality factor	Q	400
Resonant frequency	f_0	280 KHz
Tip radius	R	20 nm
Intermolecular distance	a_0	0.103 nm
Water film thickness	h	0.2 nm
Capillary force turns on	d_{on}	0.4 nm
Capillary force turns off	d_{off}	2.32 nm

In order to accurately account for these transitions during forward-time numerical simulation, one proceeds in the following manner. Given consistent and nondegenerate initial conditions $\mathbf{x}_0$ and i_0, seek a numerical approximation for the solution to the initial-value problem

$$\dot{\mathbf{x}}(t) = \mathbf{f}[\mathbf{x}(t),i_0], \quad \mathbf{x}(t_0) = \mathbf{x}_0, \quad (7)$$

until a time $t=t_1$, corresponding to a transversal zero crossing of the value of one of the event functions h associated with $i_b=i_0$ from positive to negative. To continue beyond the corresponding transition, repeat the above construction after making the substitutions $t_0=t_1$, $\mathbf{x}_0=\mathbf{x}(t_1)$, and $i_0=i_a$.

B. Numerical results

The objective of this section is to numerically investigate the oscillatory dynamics of an atomic force microscope cantilever driven by a single-frequency excitation of its clamped end for the parameter values listed in Table II. To enable some reasonable comparison, we have chosen to use the values listed in Ref. 6, corresponding to a commercially available AFM that has a silicon tip tapping a silicon surface.

A typical experimental amplitude-separation curve would be obtained by graphing a representative measurement of the extent of the cantilever oscillations as the equilibrium position of the cantilever is brought toward the sample surface and then retracted, i.e., as d_0 is decreased and subsequently increased. Assuming that the resting time subsequent to each change in the equilibrium position is sufficiently long, the post-transient cantilever response can be identified with a steady-state attractor of the corresponding dynamical system. The steady-state attractor observed subsequent to each change in equilibrium position is then a function of the basin of attraction within which lie the initial conditions obtained from the previously found attractor and, naturally, the influence of noise and uncertainty.

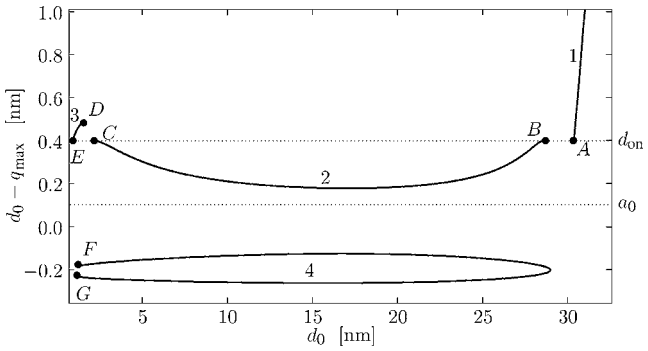

FIG. 2. Branches of periodic solutions obtained using numerical pseudo-arclength continuation. The points labeled $A-G$ correspond to periodic solutions that achieve grazing contact with a surface defined by an event function. Specifically, points A, B, C, and E represent grazing contact with the onset of capillary interactions given by the $x_1=d_0-d_{\text{on}}$ plane in state space (a dotted horizontal line is included to guide the eye). Points D, F, and G represent grazing contact with termination of the capillary force given by the $x_1=d_0-d_{\text{off}}$ plane in state space.

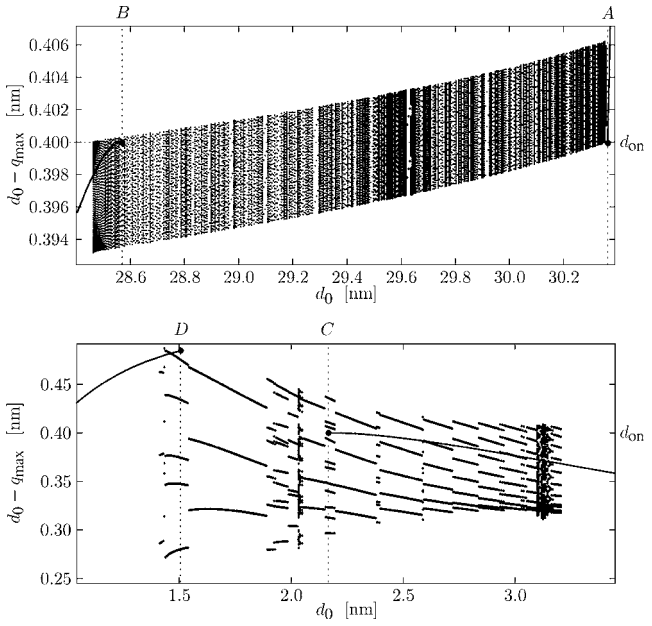

FIG. 3. Steady-state attractors found using forward-time simulation. Here, 100 values of q have been sampled after an initial transient period of 1000 cycles of the drive. Separate simulations are performed as the equilibrium separation d_0 is varied in steps of 0.005 nm. The gray solid curves on the left and right sides of the figure represent segments of branches of periodic solutions found using pseudo-arclength continuation. The upper panel corresponds to the segment between points A and B and the lower panel corresponds to the segment between points C and D shown in Fig. 2.

Both forward-time simulation and numerical continuation[18] may be employed to trace a periodic steady-state attractor as d_0 is varied. Numerical continuation is preferred due to its rapid rate of convergence, improved accuracy, and ability to continue the periodic trajectory even beyond bifurcation points characterized by a change in the linear stability. On the other hand, forward-time simulation becomes a necessary tool in the event that a branch of periodic trajectories terminates for some parameter value as we show below.

Figure 2 shows four branches of periodic steady-state solutions obtained using numerical continuation. The ordinate axis illustrates the minimum tip-sample distance during an oscillation (cf. Fig. 1).

As expected, there exists a branch of periodic solutions (labeled 1 in Fig. 2) that is independent of the sample position for sufficiently large equilibrium separations. This branch terminates at an equilibrium separation of $d_0 \approx 30.36$ nm, at which the corresponding periodic trajectory achieves *simple grazing contact* with the water layer represented by the $x_1=d_0-d_{\text{on}}$ plane in state space. A further decrease in d_0 results in the onset of capillary interactions. Since the capillary force interaction persists until the trajectory crosses the $x_1=d_0-d_{\text{off}}$ plane in state space, the corresponding perturbation to the periodic trajectory is not small. As a result, no periodic trajectory with a period equal to the drive period that includes capillary interactions is expected to emanate from this point.

To proceed beyond the onset of capillary force interactions, forward-time simulation is performed following the numerical approach discussed previously. The upper panel of Fig. 3 shows the family of steady-state attractors obtained by initializing the forward-time simulation with the grazing periodic trajectory. Here, 100 values of q are sampled at local minima (in time) in the tip-sample separation after an initial transient period of 1000 cycles of the drive. This is repeated as the value of d_0 is decreased in steps of 0.005 nm. For the case of a periodic solution with a period equal to the drive period, the data yield a single point for some particular value of d_0, whereas a scatter of points corresponds to more complex dynamics. For example, near $d_0=29.3$ nm a periodic response with a period equal to three times that of the driving force is found, whereas for $d_0=29.6$ nm the response appears highly irregular. The figure highlights the distinct difference between the pregrazing periodic trajectory and the postgrazing steady-state attractors. As an example, Fig. 3 shows that the postgrazing oscillatory dynamics is characterized by a recurrent (albeit not on every close approach) occurrence of a liquid column between the tip and the sample surface.

The family of steady-state attractors transitions to a periodic steady-state attractor at $d_0 \approx 28.46$ nm. The corresponding branch of periodic trajectories may be continued using numerical continuation both for increasing and decreasing values of d_0 (see branch 2 in Fig. 2 and the solid curve on the left side of the upper panel of Fig. 3). There thus exists an interval of values of d_0 for which the periodic trajectories coexist with the more complicated steady-state attractors. A similar observation is again made near $d_0 \approx 2.17$ nm, where the branch of periodic trajectories again terminates at a grazing trajectory (cf. the lower panel of Fig. 3). Indeed, the family of steady-state attractors that appears around $d_0 \approx 3.3$ nm persists until $d_0 \approx 1.4$ nm, where yet another branch of periodic trajectories is found (labeled branch 3 in Fig. 2). This branch corresponds to trajectories with i identically equal to 1, i.e., for which the meniscus is maintained throughout the oscillation, and terminates at either end at points corresponding to grazing periodic trajectories.

Using forward-time simulation for a large set of initial conditions in a trial and error manner, it was possible to locate and trace a second periodic steady-state attractor under

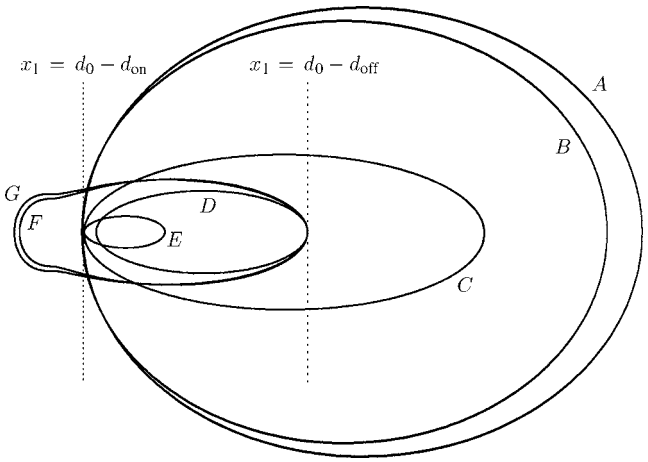

FIG. 4. Periodic solutions that achieve grazing contact with the $x_1=d_0-d_{on}$ plane (A, B, C, and E) or the $x_1=d_0-d_{off}$ plane (D, F, and G) in state space. The curves corresponding to A and B exhibit grazing contact with the d_0-d_{on} surface but have been rescaled in magnitude to fit in the figure with the other curves. Curves $C-G$ are not scaled in this way and represent the actual values.

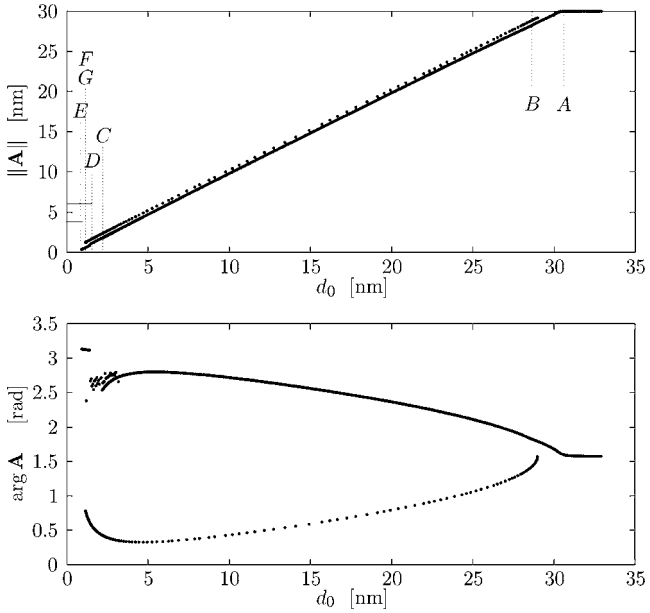

FIG. 5. Variations in magnitude $\|\mathbf{A}\|$ and phase arg $\mathbf{A}$ of the complex amplitude $\mathbf{A}$ of the frequency component of the response with frequency equal to the excitation frequency under changes in d_0. Here, a discrete fast Fourier transform has been applied to the steady-state responses found using forward-time simulation and pseudo-arclength continuation sampled 512 times per period over 20 periods of the excitation.

variations in d_0 shown as the lower segment of branch 4 in Fig. 2. As suggested by the figure, it is not possible to continue this steady-state attractor past $d_0 \approx 28.98$ nm. Instead, initial conditions on the steady-state attractor eventually converge to the original steady-state attractor as d_0 is increased beyond the critical value. The fold in the branch of periodic solutions corresponds to a saddle-node bifurcation at which two branches of periodic solutions merge. In this case, the upper branch consists of unstable periodic solutions. Both branches terminate near $d_0 \approx 1.2$ nm in grazing bifurcations shortly after additional folds and changes in solution stability.

As discussed in the previous paragraphs, each branch of periodic steady-state solutions appears to terminate at a grazing trajectory that achieves grazing contact with a state-space surface on which an associated event function equals zero. Figure 4 shows the periodic trajectories found at each of the terminal points in Fig. 2. Four of these, namely the trajectories labeled A, B, C, and E, achieve grazing contact with the state-space surface corresponding to the transition between $i_b=0$ and $i_a=1$, whereas the remaining trajectories, labeled D, F, and G, achieve grazing contact with the state-space surface corresponding to the transition between $i_b=1$ and $i_a=0$. As discussed previously, these transitions correspond to discontinuous changes in the tip-sample interaction force, an observation that can be placed on a causal footing through a rigorous analysis based on the technique of discontinuity mappings.[13,19]

While regular periodic trajectories with a period identical to that of the driving exist only in certain ranges of d_0, it is not always easy to distinguish these from the irregular or high-periodic response found in other ranges without the sampling technique introduced here. Suppose that, instead of sampling, spectral analysis is performed to extract the complex amplitude of the frequency component of the response with frequency equal to that of the driving. As shown in Fig. 5, there is an apparently continuous change in the magnitude and phase of the response calculated by this method, and no distinct trace of the irregularity of the instantaneous response for $d_0 \approx 30.36$ nm and $d_0 \approx 28.46$ nm. A similar continuous transition also appears in the magnitude for small d_0, while some irregularity is still evident in the phase.

IV. CONCLUSION

Using both forward-time simulation and numerical continuation techniques tailored specifically for use with hybrid dynamical systems, we have gained new insight into the steady-state cantilever dynamics during tapping mode atomic force microscopy. Several features of the bifurcation analysis found here are expected to generically occur in the cantilever response, although specific details will vary as to their location and extent under variations in system parameters. These include the coexistence of multiple steady-state attractors, the irregular response separating regions of periodic response, and the existence of grazing trajectories corresponding to the termination points of branches of periodic solutions. Although the property of grazing is particular to the hybrid formulation, the qualitative existence of termination points as periodic trajectories reach regions in which rapid changes occur in the vector field is expected to persist in a smoothed model.[20]

ACKNOWLEDGMENTS

We are grateful for useful interactions with Craig Prater. We also acknowledge support from National Science Foundation CMMI Grant Nos. 0510044 and 0619028.

[1]G. Binnig, C. Quate, and C. Gerber, Phys. Rev. Lett. **56**, 930 (1986).
[2]N. Jalili and K. Laxminarayana, Mechatronics **14**, 907 (2004).
[3]G. Bar, Y. Thomann, and M. Whangbo, Langmuir **14**, 1219 (1998).

[4]R. Garcia and R. Perez, Surf. Sci. Rep. **47**, 197 (2002).
[5]R. Garcia and A. San Paulo, Phys. Rev. B **60**, 4961 (1999).
[6]L. Zitzler, S. Herminghaus, and F. Mugele, Phys. Rev. B **66**, 155436 (2002).
[7]H. Dankowicz, Philos. Trans. R. Soc. London, Ser. A **364**, 3505 (2006).
[8]S. Lee, S. Howell, A. Raman, and R. Reifenberger, Phys. Rev. B **66**, 115409 (2002).
[9]S. Lee, S. Howell, A. Raman, and R. Reifenberger, Ultramicroscopy **97**, 185 (2003).
[10]N. Burnham, O. Behrendt, F. Oulevey, G. Gremaud, P.-J. Gallo, D. Gourdon, E. Dupas, A. Kulik, H. Pollock, and G. Briggs, Nanotechnology **8**, 67 (1997).
[11]K. Yagasaki, Phys. Rev. B **70**, 245419 (2004).
[12]J. Tyson and B. Novak, *Cell Cycle Controls in Computational Biology* (Springer & Business Media, Inc., New York, 2002).
[13]H. Dankowicz, X. Zhao, and S. Misra, Int. J. Non-Linear Mech. **42**, 697 (2007).
[14]S. Ciraci, E. Tekman, A. Baratoff, and I. Batra, Phys. Rev. B **46**, 10411 (1992).
[15]D. Beaglehole and H. K. Christenson, J. Phys. Chem. **96**, 3395 (1992).
[16]J. Jang, G. Schatz, and M. Ratner, J. Chem. Phys. **120**, 1157 (2004).
[17]A. Garcia-Martin and R. Garcia, Appl. Phys. Lett. **88**, 123115 (2006).
[18]B. Krauskopf, H. Osinga, and J. Galan-Vioque, *Numerical Continuation Methods for Dynamical Systems* (Canopus Publishing Ltd., Bristol, UK, 2007).
[19]H. Dankowicz and M. R. Paul, ESDA 2008, 9th Biennial ASME Conference on Engineering Systems Design and Analysis (2008).
[20]H. Dankowicz, Nonlinear Dyn. **50**, 511 (2007).